ELSEVIER

Single-phase heat transfer and flow friction correlations for microfin tubes

C. C. Wang
Energy and Resources Laboratories, Industrial Technology Research Institute, Taiwan, ROC

C. B. Chiou and D. C. Lu
Department of Mechanical Engineering, National Chiao Tung University, Taiwan, ROC

Single-phase heat transfer as well as pressure drop characteristics for microfin tubes with nominal diameter of 9.52, 7.94, and 7.0 mm are reported in the present investigation. In this study, seven commercially available microfin tubes and a smooth tube were tested using water as the test fluid. The heat transfer coefficients were obtained using the Wilson plot technique. It was found that the microfin tube exhibits a rough tube characteristics, and the enhancement levels increase with the Reynolds number and eventually reach a maximum value at a critical Reynolds number. The Dittus–Boelter type Wilson plot function cannot correlate the heat transfer data when the Reynolds number is less than the critical Reynolds number. Using the heat-momentum transfer analogy, a better correlation of the present mirocfin heat transfer data is achieved. In addition, the present correlations can predict 85.2% of the experimental data within 10% and 95.8% of the friction factor within 10%.

Keywords: microfin tube; heat-momentum analogy; single-phase; heat transfer; pressure drops; heat exchangers

Introduction

The microfin tube was first developed by Fujie et al. (1977) of Hitachi Cable. Since then, the microfin tube has been proved to be very effective in refrigeration and air-conditioning applications. One reason for the popularity of the microfin tube is the larger heat transfer enhancement relative to the increased pressure drop. For instance, a 50–100% increase in evaporation and condensation heat transfer coefficients, while only 20–50% increase in pressure drop was reported by Schlager et al. (1989). Furthermore, regarding concerns of reliability, durability, safety, and fouling, microfin tubes are essentially equivalent to plain tubes. In addition, the relatively low cost of the production of microfin tubes has significantly increased their popularity in recent years. In the past decade, two-phase performance of microfin tubes has been reported by numerous investigators. Schlager et al. (1990) reported a 2.2 enhancement ratio with R-22 in a 12.7-mm tube. Khanpara et al. (1987) indicated similar enhancement levels for evaporating refrigerants in similar tubes. They also noted a decrease of these levels with increasing mass velocity. Chiang (1993) reported both evaporation and condensing heat transfer coefficients for microfin tubes with both axial and helical configurations. His data showed that the evaporation heat transfer coefficients increase with the increase of tube diameter, while the condensing heat transfer coefficients decrease with the increase of tube diameter.

Although many investigators had devoted their efforts to studying the two-phase thermal characteristics of microfin tubes, single-phase heat transfer characteristics of the microfin tube are not well established. As is known, the single-phase heat transfer data are of special value for the subcooled region of air-cooled condensers and the superheated region of the air-conditioning evaporator. In addition, the design of water cooling/heating coils commonly used in ventilators and package air conditions, requires knowledge of the single-phase heat transfer data. Unfortunately, investigations of the single-phase heat transfer with the microfin tube in the open literature are not well correlated. For instance, the single-phase R-113 heat transfer coefficients for Khanpara et al. (1987) indicate $Nu/Pr^{0.4}$ is proportional to $Re^{1.7}$ in the Re range from 6000 to 15,000. However, their R-22 data ($12000 < Re < 15{,}000$) are well below the extension of the R-113 line. Eckels and Pate (1991) found that the single-phase heat transfer coefficients of the microfin tube are proportional to $Re^{0.8}$. Al-Fahed et al. (1993) performed a single-phase experimental study on 15.9-mm OD smooth and microfin tube using water as the test fluid. Their data also indicate that the single-phase heat transfer coefficients for a microfin tube are proportional to $Re^{0.8}$ in the range of $10{,}000 < Re < 30{,}000$. The single-phase heat transfer enhancement level of the microfin tube for previous investigators are approximately $1.2 \sim 1.8$; whereas, the pressure drop enhancement level is approximately 1.4–2.3.

Chiou et al. (1995) presented single-phase heat transfer coefficients as well as friction factors for two microfin tubes. Experiments were carried out in a double-pipe heat exchanger. They found that the microfin tube exhibits rough tube characteristics,

Address reprint requests to C. C. Wang, D200 ERL/ITRI, Bldg. 64, 195-6 Section 4, Chung Hsing Rd., Chutung, 310, Hsinchu, Taiwan, ROC.

Received 14 November 1995; accepted 19 March 1996

Int. J. Heat and Fluid Flow 17: 500–508, 1996

655 Avenue of the Americas, New York, NY 10010

0142-727X/96/$15.00
PII S0142-727X(96) 00048-1

and a maximum phenomenon of Stanton numbers was reported. In their study, they had kept the LMTD (logarithm mean temperature difference) constant in the Wilson plot method as quoted by Shah (1990). However, to apply the Wilson plot technique correctly, it is necessary to ensure that the thermal resistance within the annulus be constant. Consequently, the present study reconducted the experiments. In addition, five additional microfin tubes were tested, and a generalized correlation were proposed.

As shown above, existing data for microfin tubes seem quite ambiguous. In addition, most of the investigators do not report the heat transfer coefficients for Reynolds numbers less than 10,000. However, design of air-conditioning systems in this range is often encountered. Therefore, it is of value to clarify the single-phase heat transfer characteristics of microfin tubes for Re ~ 2,500–40,000. A total of eight tubes including seven commercially available microfin tubes and a smooth tube were tested. The detailed geometric parameters are presented in Table 1. Based on the heat-momentum transfer analogy, correlations for the Stanton number and friction factors are obtained.

Experimental setup

Experiments were carried out in a double-pipe heat exchanger as depicted in Figure 1. The test rig is made up of two independent water loops: a heating water loop in annulus and a cooling water loop inside the tube. The heating water loop consists of a 373 W pump which delivered water from a thermostat. A magnetic flow meter is installed between the pump and the test section. The magnetic flow meter was precalibrated with ±0.2% of full-scale accuracy. The cooling water loop is similar to that of the heating loop.

The test section is a horizontal double-pipe heat exchanger. The heat exchanger was well insulated by a 25-mm thick rubber material. Heat loss to the ambient was estimated to be less than ±1% of the total heat transfer rate at the lowest water flow through the test section. Hot and cold water flow through the test section countercurrently within the annulus and the test tube. The effective heat transfer length is 1200 mm. The inlet and outlet temperatures of the double-pipe heat exchanger were recorded by four RTDs (Pt100Ω) having a calibration accuracy

Notation

A_i	nominal inside heat transfer area of the tube, m^2
A_o	outside heat transfer area of the tube, m^2
$A_{i,\mathrm{tot}}$	total inside heat transfer area of the tube, m^2
A_w	mean wall surface area, evaluated as $(A_o + A_i)/2$, m^2
b	intercept of line with ordinate, K/W
B	correlation function for rough tubes, dimensionless
C_i	constant for inside heat transfer correlation, dimensionless
C_p	heat capacity of water, J/kg K
D_i	inside diameter of the tube, m
D_o	outside diameter of the tube, m
D_h	hydraulic diameter, m
e	absolute roughness (fin height), m
e^+	roughness Reynolds number, dimensionless
E	heat transfer enhancement ratio, $(h_i/h_{\mathrm{smooth}})$, dimensionless
EA	area enhancement ratio, $A_{i,\mathrm{tot}}/A_{\mathrm{smooth}}$, dimensionless
F	friction penalty factor, f_i/f_{smooth}, dimensionless
f	Fanning friction factor, dimensionless
$\bar{g}$	correlation function for rough tubes, dimensionless
h_o	heat transfer coefficient on the annulus side, W/m^2 K
h_i	inside heat transfer coefficient, based on A_i, W/m^2 K
k	thermal conductivity of water, W/m^2 K
K_{loss}	pressure loss coefficient, dimensionless
L	tube length, m
LMTD	logarithm mean temperature difference, K
m	slope of least-square deviation line, dimensionless
$\dot{m}$	average mass flow rate of coolant water, kg/s
n	Reynolds number exponent, dimensionless
n_f	number of fins
Nu	Nusselt number, $h_i D_i/k$, dimensionless
p	helical fin pitch of microfin tube, $\pi D_i/n_f \tan\alpha$, m
Pr	Prandtl number, dimensionless
ΔP	pressure drop, Pa
ΔP_{loss}	pressure drop due to change of area, Pa
Q	average heat transfer rate, W
Re	Reynolds number based on maximum inside diameter D_i, dimensionless
R_w	wall resistance, K/W
St	Stanton number, dimensionless
ΔT	temperature rise on the water coolant, K
ΔT_1	temperature difference, $\Delta T_1 = T_{i,\mathrm{in}} - T_{o,\mathrm{out}}$, K
ΔT_2	temperature difference, $\Delta T_2 = T_{i,\mathrm{out}} - T_{o,\mathrm{in}}$, K
U_o	overall heat transfer coefficient, W/m^2 K
u^*	friction velocity, m/s
V	flow velocity, m/s
X	Wilson plot function, K/W
X_b	correlation parameter, dimensionless
X_f	correlation parameter, dimensionless
X_g	correlation parameter, dimensionless
Y	Wilson plot function, K/W
y	distance from wall, m
y_b	correlation parameter, dimensionless
y_f	correlation parameter, dimensionless
y_g	correlation parameter, dimensionless

Greek

α	helix angle, degree
δ_w	wall thickness, m
η	efficiency index η $((h_i/h_{\mathrm{smooth}})/(f_i/f_{\mathrm{smooth}}))$, dimensionless
μ	dynamic viscosity of water, Pa·s
ν	kinematic viscosity of water, m^2/s
ρ	density of water, kg/m^3
τ_w	wall shear stress, Pa

Subscripts

i	tube side
in	inlet
o	annulus side
out	outlet
smooth	smooth tube surface condition
w	wall

Table 1 Geometrical parameters of test tubes

Tube #	D_o, mm	D_i, mm	D_h, mm	δ_w, mm	e,	α, °	n_f	e/D_i	p/e	$A_{i,tot}$ m^2/m	$EA=\frac{A_{i,tot}}{A_{smooth}}$	$E=\frac{Nu}{Nu_{smooth}}$	EA/E	f/f_{smooth} Re= 30,000	f/f_{smooth} Re= 10,000
1	9.52	7.92	7.92	0.8	—	—	—	—	—	0.248	1.00	1	1	1	1
2	9.52	8.96	5.61	0.28	0.20	18	60	0.0223	7.22	0.430	1.53	1.99	1.30	1.97	1.96
3	9.52	8.96	6.78	0.28	0.15	25	65	0.0167	6.19	0.360	1.28	1.63	1.27	2.29	1.96
4	9.52	8.92	5.43	0.30	0.20	18	60	0.0224	7.19	0.440	1.57	1.80	1.15	1.69	1.53
5	9.52	8.96	5.81	0.28	0.15	18	60	0.0163	9.63	0.420	1.49	1.60	1.07	1.59	1.33
6	7.94	7.38	5.13	0.28	0.15	17	65	0.0196	7.78	0.320	1.38	1.48	1.07	2.16	1.94
7	7.00	6.46	4.10	0.27	0.15	18	60	0.0232	6.94	0.305	1.50	1.83	1.22	2.12	1.84
8	7.00	6.48	3.94	0.26	0.15	18	50	0.0231	8.30	0.320	1.57	1.85	1.18	1.57	1.43

Note: the helical fin pitch p is evaluated as $\pi D_i/n_f \tan\alpha$
Nu_{smooth}: Use Equation 14 for the smooth tube
f_{smooth}: Use the present experimental data

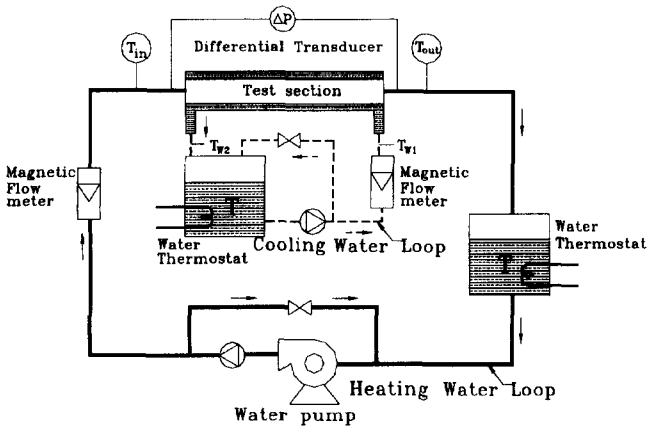

Figure 1 Schematic diagram of test apparatus

of 0.05°C. The pressure drop across the test tubes was measured by a precision differential pressure transducer, reading to ±0.1% of the test span. The energy balance between the tube side and annulus were generally within 1%. For each test run, the average fluid temperature and the average Reynolds number in the annulus of the test section were held constant to apply the Wilson plot technique correctly. This can be accomplished using an iterative procedure by simultaneously controlling the inlet temperature and the inlet water flow rate within the annulus. Experimental test conditions are shown in Table 2. As illustrated in the table, two fixed inlet temperatures (14 and 30°C) are used to determine the Prandtl number dependence of the microfin tube.

All the signals, including those from RTDs (Pt100Ω), magnetic flow meters, and differential pressure transducer, were collected and converted by a hybrid recorder. The digital signals were sent to the host computer through a GPIB interface for further operations. Uncertainties in the reported experimental values of the heat transfer coefficients, following the single-sample uncertainty analysis proposed by Moffat (1988), are presented in Table 3.

Heat transfer data reduction

The overall thermal resistance is evaluated from

$$U_o = \frac{Q}{\text{LMTD} \times A_o} \tag{1}$$

where Q is the average heat transfer rate of the annulus and tube; i.e.,

$$Q = \left(\frac{(\dot{m}Cp\Delta T)_i + (\dot{m}Cp\Delta T)_o}{2} \right) \tag{2}$$

where ΔT is the temperature rise/drop of water, and the subscripts o and i denote the annulus and tube side, respectively. In all cases, only those data that satisfy the $|(Q_o - Q_i)/Q| < 0.01$ criteria are taken into consideration in the final data reduction. The mean temperature difference LMTD is

$$\text{LMTD} = \frac{\Delta T_1 - \Delta T_2}{\ln(\Delta T_1/\Delta T_2)} \tag{3}$$

$$\Delta T_1 = T_{i,\text{in}} - T_{o,\text{out}} \tag{4}$$

$$\Delta T_2 = T_{i,\text{out}} - T_{o,\text{in}} \tag{5}$$

where $T_{i,\text{in}}$ and $T_{i,\text{out}}$ are the inlet and outlet temperatures of water in the inner tube, and $T_{o,\text{in}}$ and $T_{o,\text{out}}$ denote the inlet and outlet temperatures of water in the annulus. At the first stage, the data are analyzed by the Wilson plot method and can be described as follows.

Table 2 Test conditions

	Tube side temperature, °C	Annulus side temperature, °C	Tube side Prandtl number	Range of tube side Reynolds number for all tubes
Condition 1	14	35	7.33	2,500 ~ 35,000
Condition 2	30	45	5.38	2,500 ~ 40,000

Table 3 Summary of estimated uncertainties

Primary measurements		Derived quantities	
Parameter	Uncertainty	Parameter	Uncertainty
$\dot{m}_{annuls}$	0.5%	Re_o	0.82%
$\dot{m}_{tube}$	0.5%	Re_i	0.62%
ΔP	0.2%	f(Re=5,000)	5.2%
		f(Re=35,000)	3.2%
ΔT_i	0.1°C	j(Re=5,000)	5.9%
		j(Re=35,000)	4.9%

The experimentally determined resistance $1/UA$ of the test tube is related to individual thermal resistances as

$$\frac{1}{U_o A_o} = \frac{1}{h_o A_o} + R_w + \frac{1}{h_i A_i} \tag{6}$$

where h_o and h_i represent the average outside and inside heat transfer coefficients, and R_w denotes wall resistance and is given by $R_w = \delta_w / k_w A_w$. In the present calculation, the overall resistance is based on the outer surface area, which is evaluated as $\pi D_o L$, where D_o is the outside diameter of the inner tube. Note that the inside heat transfer coefficient is based on nominal inside surface area ($\pi D_i L$). The properties for both streams were calculated using the average of the inlet and outlet bulk fluid temperatures.

The tube side heat transfer coefficient for the smooth tube h_i is assumed to have the following form:

$$h_i = C_i \frac{k_i}{D_i} \left(\frac{\rho V D}{\mu} \right)_i^{0.8} \left(\frac{Cp\mu}{k} \right)_i^{0.4} \tag{7}$$

The correlation form does not include the viscosity ratio to account for the radial property variation, because this effect is very small for the present test range. Therefore, Equation 6 then becomes

$$\left(\frac{1}{U_o A_o} - R_w \right) = \frac{1}{C_i \frac{k_i}{D_i} \left(\frac{\rho V D}{\mu} \right)_i^{0.8} \left(\frac{Cp\mu}{k} \right)_i^{0.4} A_i} + \frac{1}{h_o A_o} \tag{8}$$

Equation 8 has the linear form

$$Y = mX + b \tag{9}$$

where

$$Y = \frac{1}{U_o A_o} - R_w \tag{10}$$

$$m = \frac{1}{C_i} \tag{11}$$

$$b = \frac{1}{h_o A_o} \tag{12}$$

$$X = \frac{1}{\frac{k_i}{D_i} \mathrm{Re}^{0.8} \mathrm{Pr}^{0.4} A_i} \tag{13}$$

Therefore, with a simple linear regression, the slope of the resulting straight line is equal to $1/C_i$. Figure 2 shows the relationships of X and Y for all the test tubes. The regression result of the smooth tube (tube #1) yields $C_i = 0.0227$ which is very close to the well-known constant 0.023 of the Dittus–Boelter correlation. Note that the exponent on Re is not necessary a constant 0.8 as shown in Equation 7, as addressed by Shah (1990); it is a function of the Prandtl number and Reynolds number; it varies from 0.78 at Pr = 0.7 to 0.9 at Pr = 100 for Re = 50,000 for a circular tube. The present authors had tried several other exponents near exponent 0.8. It seems that the difference to the final results is small, therefore a fixed exponent, 0.8, is used in the present study.

It is clear from Figure 2 that the relationships between Y and X are not linear for all the microfin tubes. If all the data are included in the analysis for any one of the microfin tubes, accompanied by an appropriate adjustment of the Reynolds number exponent, it is found that the Reynolds number exponent will range from 1.5 to 2.0. Kandlikar (1991) used Khanpara et al. (1987) single-phase heat transfer test results of R-113 in the range of 6,000 < Re < 15,000, and indicated an Re exponent of 1.7. However, including all the data for one tube in the regression is not realistic, because the relationship between Y and X is not linear in nature for microfin tubes. Nonetheless, linear relationships between X and Y were observed for microfin tubes at the higher Reynolds numbers. Therefore, using the standard Wilson plot technique to the higher Reynolds number data (corresponds to the linear part of the test microfin tubes), we found that the Nusselt number for all the test tubes can be written as:

$$\mathrm{Nu} = 0.02274 \mathrm{Re}^{0.8} \mathrm{Pr}^{0.4} \quad \text{(for tube \#1, Re > 10,000)} \tag{14}$$

$$\mathrm{Nu} = 0.0452 \mathrm{Re}^{0.8} \mathrm{Pr}^{0.4} \quad \text{(for tube \#2, Re > 13,000)} \tag{15}$$

$$\mathrm{Nu} = 0.0370 \mathrm{Re}^{0.8} \mathrm{Pr}^{0.4} \quad \text{(for tube \#3, Re > 18,800)} \tag{16}$$

$$\mathrm{Nu} = 0.04086 \mathrm{Re}^{0.8} \mathrm{Pr}^{0.4} \quad \text{(for tube \#4, Re > 17,900)} \tag{17}$$

$$\mathrm{Nu} = 0.0363 \mathrm{Re}^{0.8} \mathrm{Pr}^{0.4} \quad \text{(for tube \#5, Re > 18,800)} \tag{18}$$

$$\mathrm{Nu} = 0.03365 \mathrm{Re}^{0.8} \mathrm{Pr}^{0.4} \quad \text{(for tube \#6, Re > 20,400)} \tag{19}$$

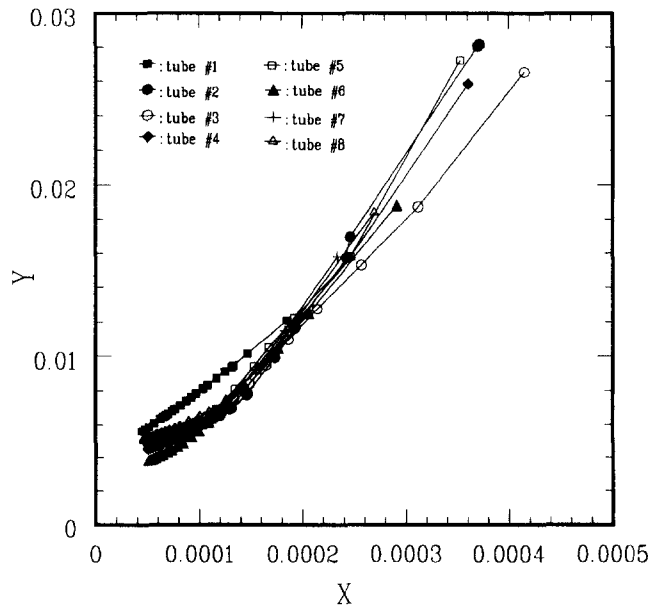

Figure 2 Wilson plot results for tested tubes

$$Nu = 0.04165Re^{0.8}Pr^{0.4} \quad \text{(for tube \#7, Re > 18,000)} \quad (20)$$

$$Nu = 0.04198Re^{0.8}Pr^{0.4} \quad \text{(for tube \#8, Re > 19,000)} \quad (21)$$

Note that the characteristic length of the Nusselt number and Reynolds number in Equations 14–21 is based on the maximum inside diameter of the microfin tubes. The applicability of Equations 14–21 is valid for higher Reynolds numbers, as indicated, which corresponds to mass velocities that are generally greater than 200 kg/m^2·s. However, for air-conditioner design, mass flux between 100 ~ 200 kg/m^2 s (Re = 6,500 ~ 13,000, corresponding values of X in Figure 2 are 0.00022–0.00012) are often encountered. Therefore, it is important to obtain the heat transfer correlation that is applicable to the whole test range. To obtain the heat transfer coefficients in the whole test range, a modified Wilson plot technique must be made. As outlined by Shah (1985), procedures for obtaining the heat transfer coefficients can be described as follows:

(1) using the Wilson plot technique addressed previously in the linear range to obtain the intercept, $b = 1/h_o A_o$, which is constant throughout the experiments; and
(2) using Equation 6 and the intercept b to back out the inside heat transfer coefficients for the whole test range.

As a result, the inside heat transfer coefficients can be obtained as long as the thermal resistance in the annulus was kept unchanged. Actually, all the experimental data presented in this study use this analyzing approach. As addressed previously, the nonlinear characteristics of Wilson plot graph suggests that the correlation form of Nu(Re, Pr) for microfin tubes may not be appropriate to cover the entire test range. Accordingly, a correlation based on heat-momentum transfer analogy is proposed later to correlate all the experimental data.

Pressure drop data reduction

Pressure drop measurements were performed without heat addition to the test section. The friction factor for the test tubes can be obtained from the Fanning friction factor equation.

$$f = \frac{D_i}{4L}\left[\frac{\Delta P - \Delta P_{loss}}{\left(\frac{1}{2}\rho V^2\right)}\right] \quad (22)$$

where $\Delta P_{loss} = K_{loss}(\rho V^2/2)$, which accounts for the entrance and exit pressure losses due to the connection of the test tube and the plain end fittings. The loss coefficient K_{loss} taken from Idelchik (1994), is approximately equal to 0.05 for the present test condition. The fractions of the evaluated ΔP_{loss} to the measured pressure drop for microfin tubes are less than 1% and 2.4% for a smooth tube.

Results and discussion

Figure 3 compares the smooth tube test results of the heat transfer and friction factors data. The ordinate shown in the figure is in the form of Nu/Pr$^{0.4}$. As seen in the figure, there is a good agreement between the present data and accepted correlations. The experimental results for heat transfer data agree very well with the Dittus–Boelter correlation for Reynolds number greater than 10,000, and show a detectable deviation for Re ≤ 9,000. The discrepancy between the experimental data and the Dittus–Boelter correlation is because the Dittus–Boelter correlation is valid for higher Reynolds numbers (generally greater than 10,000). In fact, Kays and Crawford (1993) suggest that the Dittus–Boelter correlation is no longer recommended. Bhatti

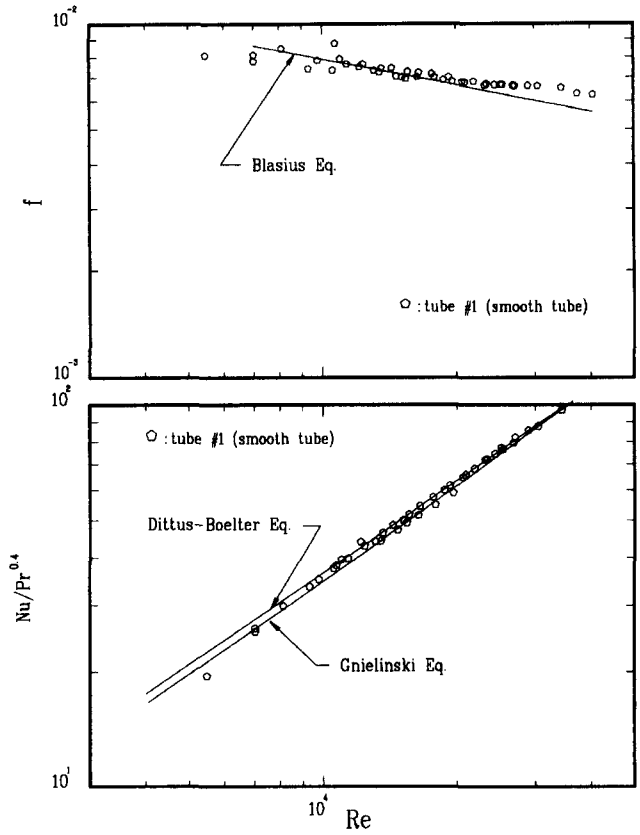

Figure 3 Test results for the smooth tube

and Shah (1987) also illustrate that predictions of the Dittus–Boelter correlation are unacceptable, because the deviations increase significantly for Re < 10,000. The overpredictions of the Dittus–Boelter correlation are up to 94% for Re = 2,500 and 0.7 ≤ Pr ≤ 120. The Gnielinski (1976) correlation, which correlates the available data over the range of Prandtl number from 0.5 to 2,000 and the Reynolds number from 2300 to 5 × 10^6, gives the best agreement with the existing data. Accordingly, the Gnielinski correlation is drawn in the figure, and an improved agreement with the experimental data is reported for Re < 10,000. The comparison between the experimental friction factors and the Blasius solution is also shown in the figure. The friction factors are in good agreement with the Blasius equation at the Reynolds number from 7,000 to 25,000, and higher by about 8% at a Reynolds number of 40,000.

Correlations of the microfin tubes

Figure 4 presents the heat transfer coefficients and the friction factors for the microfin tubes. The heat transfer coefficients are in terms of the Colburn j factor, and are given by

$$j = \frac{h_i}{(\rho V)_i Cp_j} Pr^{2/3} \quad (23)$$

As is shown in the figure, the friction factors for the microfin tubes exhibit an apparent rough pipe characteristics. Ito and Kimura (1979) also reported that the friction factors of microfin tubes for water flow were very similar to rough tubes. For rough tubes, the turbulent flow friction factors depend on the type of roughness, roughness height e relative to the pipe diameter D_i and other types of geometrical dimensions for two- and three-

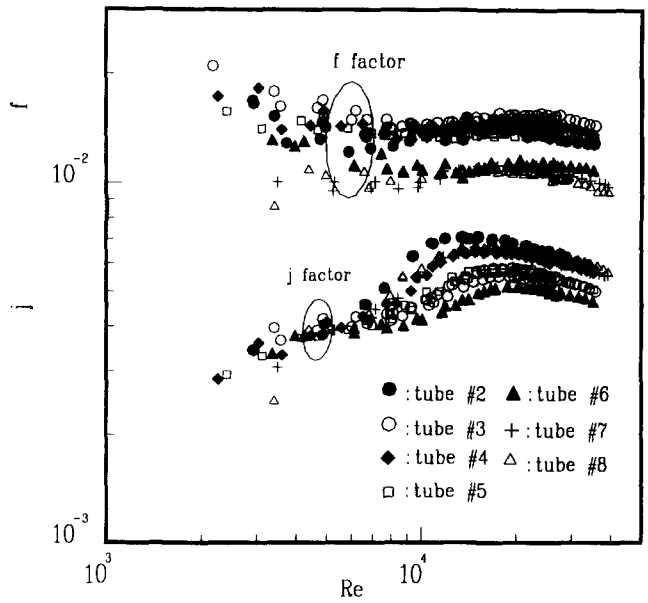

Figure 4 Experimental friction factor *versus* Reynolds number

dimensional (2-D and 3-D) roughnesses. The results are generally correlated in terms of a roughness Reynolds number e^+, defined by

$$e^+ = \frac{eu^*}{\nu} = \frac{e(\tau_w/\rho)}{\nu} = (e/D_i)\mathrm{Re}\sqrt{\frac{f}{2}} \tag{24}$$

Here u^* is referred as the "friction velocity" and e is the microfin height. The present experimental data indicate that the friction factors are relatively independent of Reynolds number when the Reynolds number is higher than 10,000, this corresponds to a roughness Reynolds number of 23 ~ 30. Thus, the results indicate that the microfin tubes show an earlier achievement of the fully rough region which starts at an e^+ of 70 for smooth tube.

Nikuradse (1933) correlated the velocity profile for $y/e > 1$ in the form

$$\frac{\bar{u}}{u^*} = -2.51\ln\left(\frac{y}{e}\right) + B(e^+) \tag{25}$$

where $B(e^+)$ is the dimensionless velocity at the tip of the roughness element corresponding to $y/e = 1$. The friction factor is obtained by integrating the velocity profile over the flow area, and for a circular tube yields:

$$\frac{\bar{u}}{u^*} = \left(\frac{2}{f}\right)^{1/2} = -2.5\ln\left(\frac{2e}{D_i}\right) - 3.75 + B(e^+) \tag{26}$$

Dipprey and Sabersky (1963) show that their sandgrain-type roughness in a circular tube may be correlated by the heat-momentum transfer analogy, which is given by

$$St = \frac{\frac{f}{2}}{1 + \sqrt{\frac{f}{2}}\left[\bar{g}(e^+)\mathrm{Pr}^n - B(e^+)\right]} \tag{27}$$

The $\bar{g}(e^+)$ function can be backed out from Equation 27 provided $B(e^+)$ is known. Equation 27 was used to correlate both the transverse and helical rib tubes with success. Webb et al. (1971) showed that Equation 27 is also applicable to 2-D roughness. They suggested that the heat-momentum transfer analogy should be applicable to any basic roughness type. Both the $\bar{g}(e^+)$ and $B(e^+)$ functions will be different for different roughness types. Recently, Webb (1994) has compiled a chronological listing of relevant references that provide experimental heat transfer data for various roughnesses, including transverse-rib roughness, integral-rib roughness, corrugated tube roughnesses, and wire coil inserts.

In the present investigation, the basic form of the heat-momentum transfer analogy correlation (Equation 27) was used to correlate the microfin tube data in the whole test range. The microfin tubes are somewhat like helical ribs with a larger number of rib starts having a lower fin height. Therefore, additional correlation parameters such as number of fins (n_f) and helical angle (α) may appear in the correlation in order to correlate all the microfin tubes tested. The correlated B function for the present seven microfin tubes for the whole test data is given as

$$B(e^+) = \exp(y_b)X_b \tag{28}$$

where

$$y_b = 2.45805 - 0.98726\ln e^+ \tag{29}$$

$$X_b = \mathrm{Re}\left(\frac{e}{D_i}\right)\left(\frac{\cos\alpha}{n_f^{0.7}}\right) \tag{30}$$

and the $\bar{g}$ function for the whole test data is given as

$$\bar{g}(e^+) = y_g X_g \tag{31}$$

where

$$X_g = \frac{n_f(\tan\alpha)^{0.1}}{(e/D_i)^{0.4}} \tag{32}$$

$$y_g = 0.007705 + 0.321(\ln e^+)/e^+ \qquad \text{for } e^+ \le 23 \tag{33}$$

$$y_g = 0.06501 - 0.51903/e^+ + 5.5956/(e^+)^2 \qquad \text{for } e^+ > 23 \tag{34}$$

As illustrated by Webb (1994), the rough surfaces show a significantly different Prandtl number dependency than a smooth tube. The present investigation shows that the Prandtl number exponent n in Equation 27 is 0.59. Note that the Prandtl number dependence is similar to those found by Brognaux (1995) (0.57), Metha and Raja Rao (1988) (0.55), Raja Rao (1988) (0.55) and Sethumadhavan and Raja Rao (1986) (0.55). The present microfin tube data show that the roughness Reynolds number $(e/D_i\,\mathrm{Re}\sqrt{f/2})$ can be correlated as a function of Re and the enhancement dimensions (e, n_f, α).

$$e^+ = 0.1407 + 0.093675X_f + 0.58464/\ln(X_f) \qquad \text{for } e^+ \le 23 \tag{35}$$

$$e^+ = 0.07313 + 0.09571X_f \qquad \text{for } e^+ > 23 \tag{36}$$

Where the correlation parameter, X_f, is given by

$$X_f = \mathrm{Re}\left(\frac{e}{D_i + \lambda}\right)\frac{n_f^{0.25}}{(\cos\alpha)^{0.5}} \tag{37}$$

and λ is a dimensional constant, which is determined from the best-fit results. The choice of λ is strictly empirical. It is also found that, without the inclusion of λ, very large overpredictions (30 ~ 100%) of the correlation are encountered. In this study, λ is found as 0.005 m for SI units.

Procedures for calculation the friction factor and Stanton number are as follows.

(1) Calculate X_f using Equation 37.
(2) Calculate e^+ from Equations 35–36.
(3) Obtain friction factor f from Equation 24.
(4) Calculate $B(e^+)$ from Equations 28–30.
(5) Calculate $\bar{g}(e^+)$ from Equations 31–34.
(6) Obtain Stanton number from Equation 27.

Note that Equations 28–37 are correlated with the Reynolds number from 2,500 to 40,000.

Experimental f values *versus* predicted value are shown in Figure 5. As seen, the present correlation (Equations 24, 35–37) can predict 95.8% of the microfin tube data within ±10%.

Figure 6 shows the experimental f factor *versus* the roughness Reynolds number (e^+) for the tested tubes. The predicted value of the present correlation is also shown in the figure. It is found from the figure that the j factors first increase with the roughness Reynolds number and reach a maximum value at a critical roughness Reynolds number and then level off beyond the maximum value. It is interesting to know that the j factors for all tested microfin tubes reach the maximum value in the range of roughness Reynolds number approximately from 23 to 30, and beyond this critical roughness Reynolds number, a linear relationship between roughness Reynolds number and j factors is noted. This suggests that the traditional Wilson plot technique is valid (Equations 14–21) for $e^+ > 30$ for the microfin tubes. Figure 7 compares the experimental data and the prediction by Equations 27–37. As shown, 85.2% of the experimental Stanton number are correlated within ±10%.

To quantify the performance of the microfin tubes, a heat transfer enhancement factor E, $(h_i/h_{\mathrm{smooth}})$, a friction penalty factor F, $(f_i/f_{\mathrm{smooth}})$, and the efficiency index η

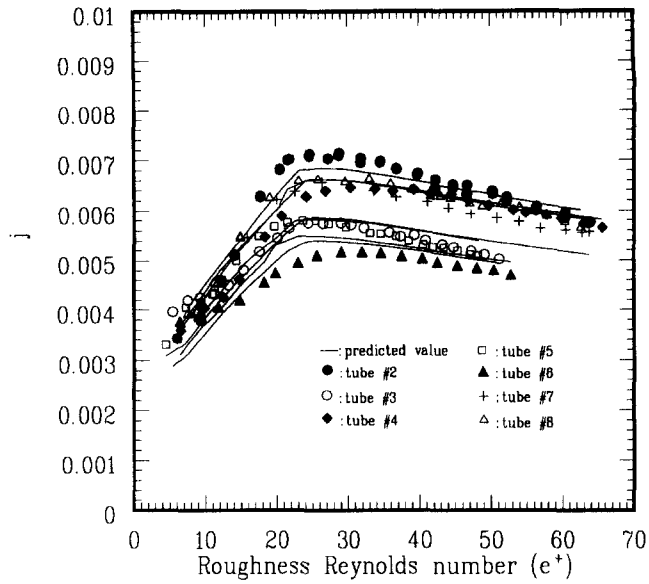

Figure 6 Heat transfer characteristics of the microfin tubes

$(h_i/h_{\mathrm{smooth}})/(f_i/f_{\mathrm{smooth}})$ are defined. These factors give the ratios of heat transfer, friction, and the increase of heat transfer coefficients over the increase in friction factors relative to the smooth tube; here h_i and f_i for microfin tubes are based on the smooth tube surface area. Figure 8 presents these factors *versus* the Reynolds number for all tested tubes. Note that the baseline of the smooth tube values; i.e., h_{smooth} and f_{smooth}, are evaluated using the Gnielinski and Blasius correlations, respectively. As seen in the figure, the heat transfer enhancement level is less than 1.2 for Re < 6,000. This indicates that the thermal boundary layer in this region is not effectively disturbed by the microfins. The enhancement ratio then shows a significant increase at 6,000 < Re < 13,000. In this region, the thermal boundary layer is becoming thinner, and the microfins begin to take into effect, which results in a significant increase. The heat transfer enhancement factor eventually reaches an asymptotic value at higher Reynolds numbers. A possible explanation of the asymptotic behaviors of the heat transfer characteristics is that at

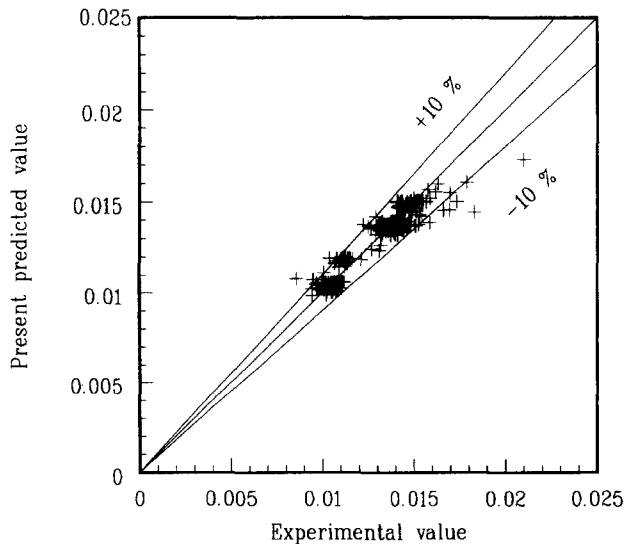

Figure 5 Experimental friction factor *versus* predicted value of the present correlation of Equations 24, 35, 36, and 37

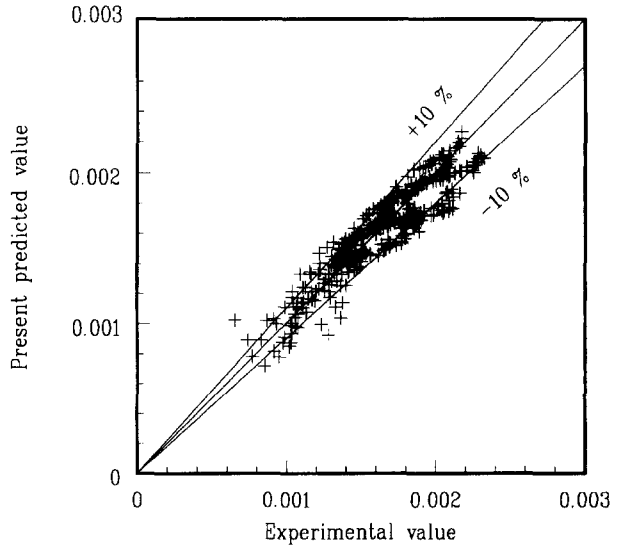

Figure 7 Experimental Stanton number *versus* predicted value of the present correlation

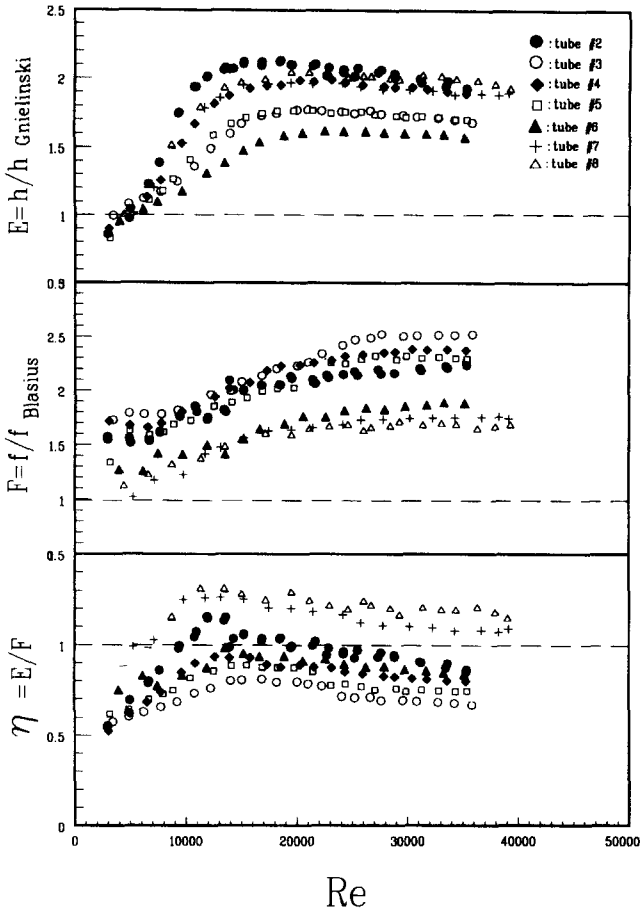

Figure 8 Heat transfer enhancement factor, friction penalty factor, and efficiency index for the test microfin tubes

higher Reynolds number the turbulence effect in microfin tubes is similar to that in a smooth tube. Al-Fahed et al. (1993) also report a similar phenomenon. The asymptotic values of the heat transfer enhancement level are between 1.47 to 1.97 as shown in Table 1. Table 1 also indicates that the enhancement level of the heat transfer coefficient is approximately 7–30% when the effect of increase surface area is taken out. Compared to the heat transfer enhancement level, the increasing rate of the friction penalty factor decreases with the increasing of the Reynolds number. Generally, the heat transfer enhancement level increases with e/D_i. The efficiency index η is an index for an enhanced tube to show the increase in heat transfer coefficient relative to the increase in friction factor. As seen from the figure, only tubes #2, #7, and #8 show an efficiency index greater than unity, and tube #7 and #8 are generally above unity. Note that tubes #7 and #8 have a smaller tube diameter (7 mm) than others. In addition, tubes #7 and #8 give the highest inside surface enhancement ratio and the highest e/D_i.

Figure 9 shows a comparison of Nusselt numbers of the present correlations (Equations 27–37) and the R-113, R-22 data from Khanpara et al. (1987) and water data from Al-Fahed et al. (1993). The tested tube by Khanpara et al. had 8.83-mm inside diameter, 60 fins, 0.22-mm fin height, and 17° helix angle, and the tube configuration of Al-Fahed et al. (1993) had a 14.8-mm inside diameter, 70 fins, 0.3-mm fin height, and 18° helix angle. As seen from the data of R-113, the enhancement level significantly decreases for Re < 10,000. This phenomenon is identical to the present test results. The proposed correlation gives an excellent agreement with the R-113 data. Again, the present correlation is in good agreement with both R-22 and water data.

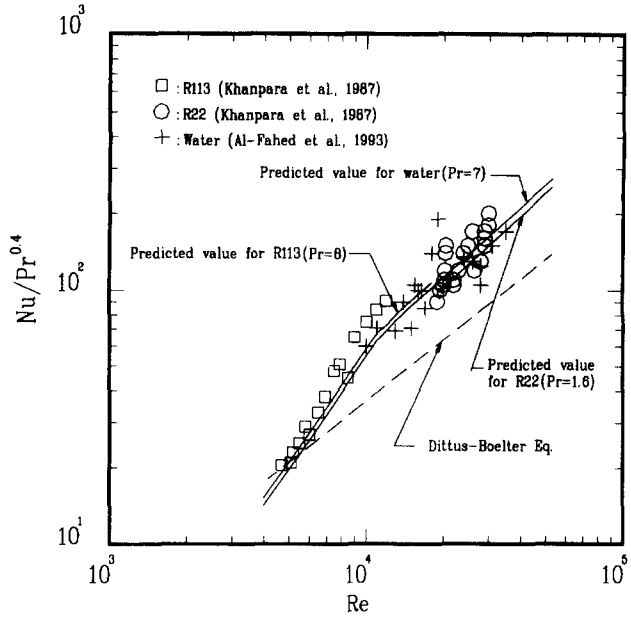

Figure 9 Comparison of the Nusselt numbers among the present correlation and Khanpara et al. (1987) data and Al-Fahed et al. (1993) data using R-113, R-22, and water as test fluids

Figure 10 compares the present correlations (Equations 27–37) with the Brognaux (1995) data at various Prandtl numbers. The specific tube tested by Brognaux had 14.83-mm inside diameter, 78 fins, 0.35-mm fin height, and 17.5° helix angle. Again, the present heat transfer correlation for Nusselt numbers provides an excellent agreement with the Brognaux data for various Prandtl number of 7.85, 6.8, and 4 and are approximately 10–30% higher for a Prandtl number of 0.7. The higher deviation between the proposed correlation and the experimental data for air may be because the present data are for water, which has a much higher value of the Prandtl number.

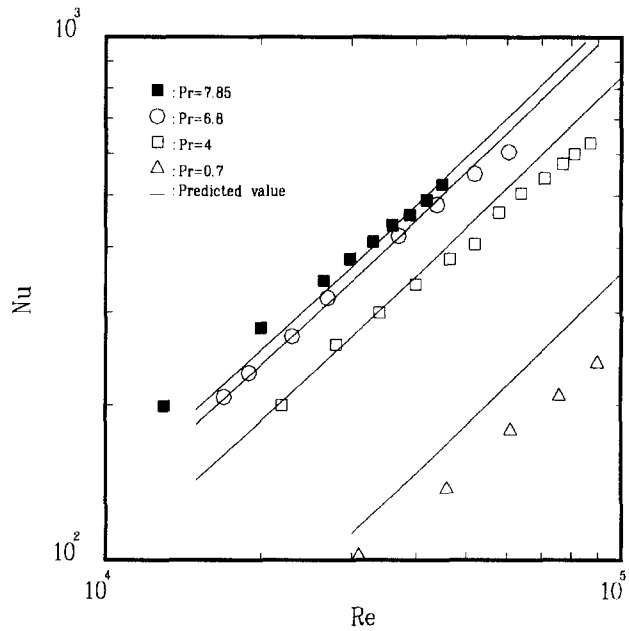

Figure 10 Comparison of the Nusselt numbers between the present correlation and Brognaux's (1995) data at various Prandtl numbers

Summary

Single-phase heat transfer and pressure drop characteristics for seven commercial available microfin tubes are reported in the present investigations. Experiments were conducted in a double-pipe heat exchanger with water as the test fluid. The heat transfer coefficients for the test tubes were obtained from the modified Wilson plot technique. For the microfin tubes, the Dittus–Boelter type correlation is valid only for the higher Reynolds numbers. For the lower Reynolds numbers, the roughness Reynolds number indicates that the flow is in the "transition region." As a result, it is suggested that the heat-momentum transfer analogy be used to correlate the single-phase heat transfer data rather than the Dittus–Boelter type equation. In the range of $2{,}500 < Re < 40{,}000$, the proposed heat transfer correlation (Equations 27–34) can predict 85.2% of the microfin data within 10%, and 95.8% of the friction factors (Equations 35–37) within 10%. In addition, the present heat transfer correlation can predict existing single-phase microfin data with reasonable accuracy.

Acknowledgments

The authors would like to express gratitude for the Energy R&D foundation funding from the Energy Commission of the Ministry of Economic. The authors are indebted to Klaus Menze at Wieland-Werke AG for providing the microfin tubes. The valuable suggestions and information from Ralph Webb are very much appreciated.

References

Al-Fahed, S. F., Ayub, Z. H., Al-Marafie, A. M., and Soliman, B. M. 1993. Heat transfer and pressure drop in a tube with internal microfins under turbulent water flow conditions. *Exp. Thermal Fluid Sci.*, **7**, 249–253

Bhatti, M. S. and Shah, R. K. 1987. Turbulent and transition flow convective heat transfer in ducts. In *Handbook of Single-Phase Convective Heat Transfer*, S. Kakac, R. K. Shah and W. Aung (eds.), Wiley Chap. 4, 32

Brognaux, L. J. 1995. Single-phase heat transfer in micro-fin tubes. Master's thesis, Dept. of Mechanical Eng., Pennsylvania State University, College Station, PA, USA

Chiang, R. 1993. Heat transfer and pressure drop during evaporation and condensation of refrigerant-22 in a 7.5-mm diameter axial and helical grooved tubes. *AIChE Symp. Series*, **89**, 205–210

Chiou, C. B., Wang, C. C., and Lu, D. C. 1995. Single phase heat transfer and pressure drop characteristics of microfin tubes. *ASHRAE Trans.*, **101**, part 2, 1041–1048

Dipprey, D. F. and Sabersky, R. H. 1963. Heat and momentum transfer in smooth and rough tubes at various Prandtl numbers. *Int. J. Heat Mass Transfer*, **6**, 329–353

Eckels, S. J. and Pate, M. B. 1991. An experimental comparison of evaporation and condensation heat transfer coefficients for HFC-134a and CFC-12. *Int. J. Refrig.*, **14**, 70–77

Fujie, K., Itoh, N., Innami, T., Kimura, H., Nakayama, N. and Yanugidi, T. 1977. *Heat Transfer Pipe*, US Patent 4044797, assigned to Hitachi Ltd.

Gnielinski, V. 1976. New equation for heat and mass transfer in turbulent pipe and channel flow. *Int. Chem. Eng.*, **16**, 359–368

Idelchik, I. E. 1994. *Handbook of Hydraulic Resistance*, 3rd. ed., Chapters 3 and 4 CRC Press

Ito, M. and Kimura, H. 1979. Boiling heat transfer and pressure drop in internal spiral-grooved tubes. *Bull. JSME*, **22**, 1251–1263

Kandlikar, S. G. 1991. A model for correlation flow boiling heat transfer in augmented tubes and compact evaporators. *J. Heat Transfer*, **113**, 966–972

Kays, W. M. and Crawford, M. E. 1993. *Convective Heat and Mass Transfer*, McGraw-Hill, New York, 319

Khanpara, J. C., Pate, M. B. and Bergles, A. E. 1987. Local evaporation heat transfer in a smooth tube and a microfin tube evaporation using refrigerants 22 and 113. In *Boiling and Condensation in Heat Transfer Equipment*, E. G. Ragi (ed.), HTD-Vol. 85, ASME, New York, 31–39

Metha, M. H. and Raja Rao, M. 1988. Analysis and correlation of turbulent flow heat transfer and friction coefficients in spirally corrugated tubes for steam condenser application. *Proc. 1988 National Heat Transfer Conference*, HTD-Vol. 96, ASME, New York, 307–312

Moffat, R. J. 1988. Describing the uncertainties in experimental results. *Exp. Thermal Fluid Sci.*, **1**, 3–17

Nikuradse, J. 1933. Laws of flow in rough pipes. (VDI Forschungsheft), English translation, NACA TM-1292 (1965)

Raja Rao, M. 1988. Heat transfer and friction correlations for turbulent flow of water and viscous nonNewtonian fluids in single-start spirally corrugated tubes, *Proc. 1988 National Heat Transfer Conference*, HTD-Vol. 96, ASME, New York, 677–683

Schlager, L. M., Pate, M. B. and Bergles, A. E. 1989. Heat transfer and pressure drop during evaporation and condensation of R-22 in horizontal micro-fin tubes. *Int. J. Refrig.*, **12**, 6–14

Schlager, L. M., Pate, M. B. and Bergles, A. E. 1990. Evaporation and condensation heat transfer and pressure drop in horizontal, 12.7-mm micro-fin tubes with refrigerant 22. *J. Heat Transfer*, **112**, 1041–1047

Sethumadhavan, R. and Raja Rao, M. 1986. Turbulent flow friction and heat transfer characteristics of single- and multi-start spirally enhanced tubes. *J. Heat Transfer*, **108**, 55–61

Shah, R. K. 1985. Heat exchangers. In *Handbook of Heat Transfer Applications*, W. M. Rohsenow, J. P. Hartnett and E. N. Ganic, (eds.), 2nd. ed. McGraw-Hill, New York, Chap. 4, 211

Shah, R. K. 1990. Assessment of modified Wilson plot techniques for obtaining heat exchanger design data. *Proc. 9th Int. Heat Transfer Conf.*, **5**, 51–56

Webb, R. L. 1994. *Principles of Enhanced Heat Transfer*. Wiley, New York, 241–242

Webb, R. L., Eckert, E. R. G. and Goldstein, R. J. 1971. Heat transfer and friction in tubes with repeated-rib roughness. *Int. J. Heat Mass Transfer*, **14**, 601–617